THE ASTROPHYSICAL JOURNAL, 337:342–354, 1989 February 1

APERTURE SYNTHESIS OBSERVATIONS OF THE 21 CENTIMETER ZEEMAN EFFECT TOWARD ORION A

T. H. TROLAND
Physics and Astronomy Department, University of Kentucky
C. HEILES
Astronomy Department, University of California, Berkeley
AND
W. M. GOSS
National Radio Astronomy Observatory and Kepteyn Astronomical Institute
Received 1988 March 17; accepted 1988 July 12

ABSTRACT

The VLA has been used to map the 21 cm Zeeman effect at 40″ resolution in the absorbing H I gas in front of Orion A. Two such regions exist having typical velocities of 1 and 5 km s^{-1}; both almost certainly lie close to the H II region. Field strengths exceed 100 μG in this H I gas. The field in the higher velocity component has been reliably detected across most of the continuum source. No field reversals exist. The distribution of line-of-sight field strengths derived for this component mimics that of τ_{HI} for positions where the lines are not saturated, suggesting that the mass-to-flux ratio in this gas is approximately constant. We have also rederived the distribution of visual extinction across Orion A using existing radio and optical data. Maxima and minima of extinction are generally coincident with maxima and minima of magnetic field. This correspondence suggests that the observed association between field strength and τ_{HI} is a real column density effect, that the effect encompasses all neutral gas in front of the source, and that the mass-to-flux ratio for this neutral gas is approximately constant. Results for Orion A lend weight to the conclusion that magnetic fields play a crucial role in the dynamics of interstellar material.

Subject headings: nebulae: individual (Orion A) — radio sources: 21 cm radiation — Zeeman effect

I. INTRODUCTION

Among the most intensively studied interstellar locales in the Galaxy, the Orion region consists of a large envelope of H I gas ($\geq 10^5\ M_\odot$, Gordon 1970), several large molecular cloud complexes ($\approx 10^5\ M_\odot$ each, Maddalena *et al.* 1986), H II regions, and dark clouds. This region, situated 150 pc below the Galactic plane, is also permeated by a magnetic field known to have structure on many size scales.

Indications of large-scale structure in the Orion magnetic field ($\geq 10°$ or 100 pc) come from the optical polarization studies of Mathewson and Ford (1970) and of Appenzeller (1974). A different perspective on the Orion magnetic field is offered by Heiles's (1987*a*, *b*) H I Zeeman effect map covering a 4° × 6° area at 30′ resolution. These data reveal field strengths of 10 μG or less in the H I envelope associated with the molecular complex. On smaller scales (≤ 1 pc), Verschuur (1969) and Brooks, Murray, and Radhakrishnan (1971) detected the Zeeman effect in the H I absorbing region in front of Orion A. This result implies a line of sight of -50 μG. (Negative values are for field lines pointed *toward* the observer.) More recently, Crutcher and Kazès (1983) and Heiles and Stevens (1986) reported the Zeeman effect in OH absorption lines toward Orion B. The former group interpreted their result as an indication of a line-of-sight field strength of $+38$ μG in front of this source. Most recently, Troland, Crutcher, and Kazès (1986) detected the Zeeman effect in the OH absorption spectrum of Orion A, with a derived field of -125 μG.

In this paper we report the application of aperture synthesis techniques to study magnetic fields in the Orion region on still smaller angular scales. We have used the Very Large Array (VLA) of the national Radio Astronomy Observatory[1] to map the Zeeman effect in the H I absorbing regions in front of Orion A on angular scales as small as 40″. This study represents the second interstellar region for which aperture synthesis Zeeman effect techniques have been applied. Previously, Schwarz *et al.* (1986) mapped magnetic field structure in the H I gas toward Cas A with the Westerbork Synthesis Radio Telescope (WSRT). Both studies provide information about small-scale variations in magnetic field strength and about the relationship between these variations and gas column densities along the lines of sight to the two continuum sources.

II. DATA ACQUISITION AND ANALYSIS

Instrumental parameters for this study are given in Table 1. In Figure 1 we present the continuum map of Orion A at the full resolution of 25″. The total flux density in this map is 390 Jy, equal to the single dish flux density for the source. (See the summary of single dish flux measurements presented by Terzian and Parish 1970.) The peak brightness temperature in Figure 1 is 4950 K, less than the estimated electron temperature of 8500 K (Wilson and Jäger 1987) since the source is not optically thick at 21 cm. The continuum map of Figure 1 has been cleaned, as have the spectral line maps used to compute H I optical depths (§ III).

Measurement of the Zeeman effect amounts to the detection of weak circular polarization. The VLA is sensitive to circular polarization, and the sense of this polarization can be inverted

[1] The National Radio Astronomy Observatory is operated by Associated Universities, Inc., under contract to the National Science Foundation.

TABLE 1

INSTRUMENTAL PARAMETERS FOR VLA 21 CM ZEEMAN SYNTHESIS OF ORION A

Parameter	Value
Array configuration	C array with 18 telescopes
Date of observation	1981 Nov
Duration of observation	9 hr
Baselines	78–1800 m
Synthesized beam width	25″
Map center	$\alpha[1950] = 05^h32^m50^s.0$ $\delta[1950] = -05°25'36''.12$
Amplitude and phase calibration	0531+194 $\alpha[1950] = 05^h31^m47^s.357$ $\delta[1950] = 19°25'24''.75$
Flux density calibration	0531+194 (6.2 Jy)
Number of spectral channels	31
Spectral resolution	3.05 kHz (0.64 km s^{-1})
Velocity coverage	13.7 to −5.7 km s^{-1}

with front end switches. We switched polarization sense every 4 minutes during the observations. Therefore, at any given time all telescopes in the array received *either* right or left circular polarization. This observing technique is quite different from the one employed at the WSRT for H I Zeeman effect studies toward Cas A (Schwarz *et al.* 1986). At the WSRT, circular polarizations were derived by cross correlating outputs from the dual linearly polarized feeds of each telescope, a procedure which results in sensitivity to both circular polarizations senses at all times.

The first step in creating a Zeeman effect map for Orion A is the extraction of Stokes parameter I and V spectra from the synthesis. The I and V spectra extracted for this purpose come from *un*cleaned maps. Examples of these spectra are shown in histogram format in Figure 2 for the pixel at the map center. (The spectra of Fig. 2 come from maps smoothed to 40″ resolution as described in § III.) From such spectra, the magnetic field follows from the ratio of V to the frequency deriv-

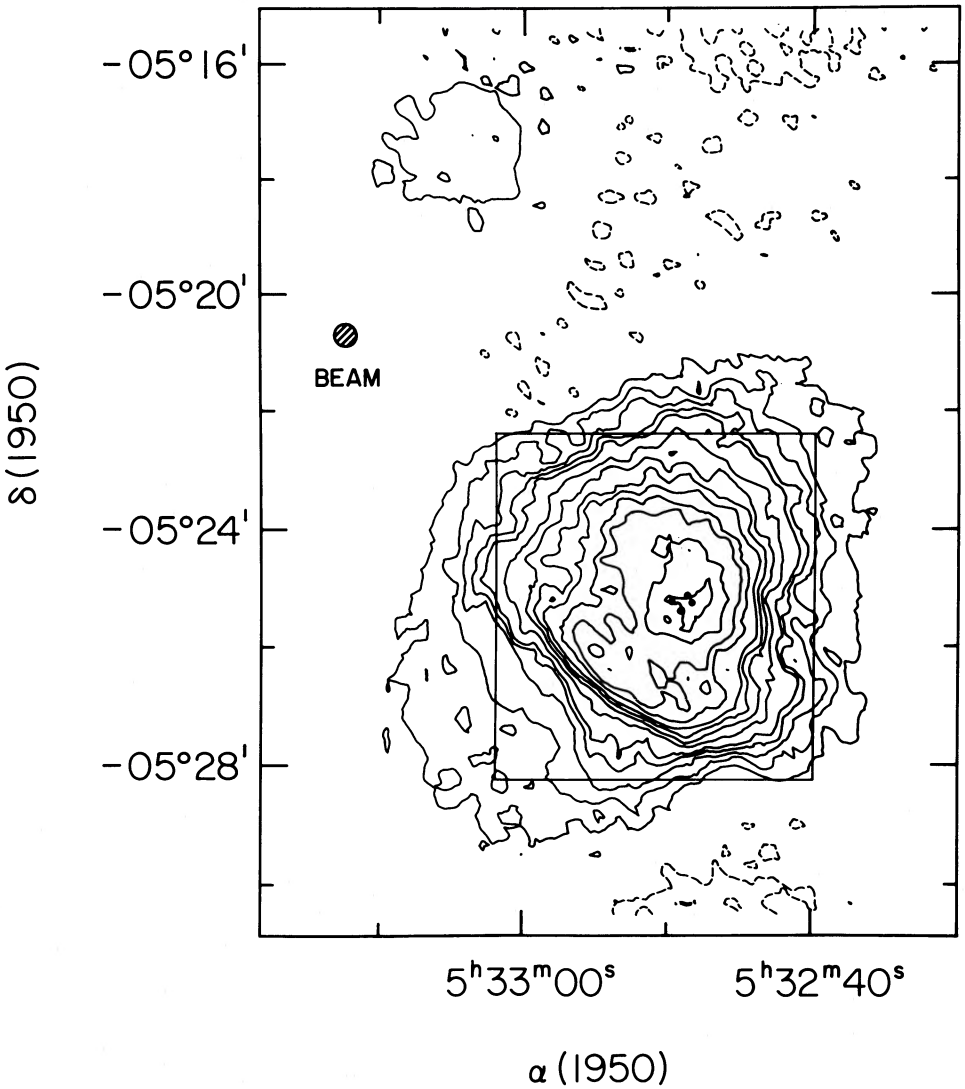

FIG. 1.—The 21 cm continuum map of Orion A at full resolution (25″) in units of Jy per beam area. Contour intervals are −0.10 (*dashed line*), 0.10, 0.20, 0.30, 0.40, 0.50, 0.75, 1.00, 1.25, 1.50, 2.00, 2.50, 3.50, and 4.50. The peak flux density is 5.05 Jy per beam area which corresponds to a brightness temperature of 4950 K, the total flux density in the map is 390 Jy. The cross hatched circle represents the synthesized beam. The four filled circles represent the Trapezium stars, θ^1 Orionis; the rectangular box denotes the field displayed in Figs. 3, 4, 5, 6, 7, and 9. The closed contour in the northeast corner of the map is NGC 1982 (M43).

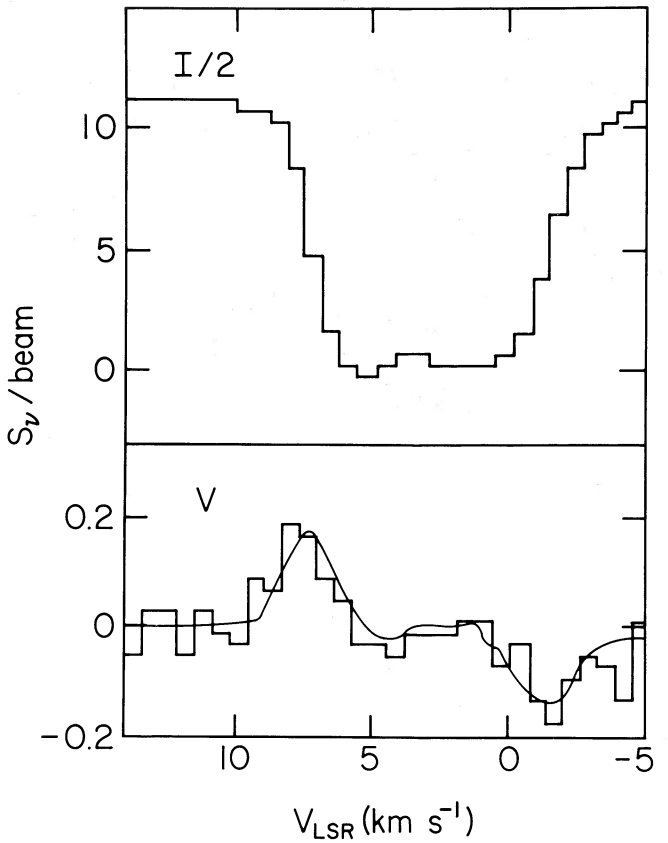

FIG. 2.—Stokes parameter $I/2$ spectrum (*top*) and V spectrum (*bottom*, histogram) for the pixel at map center, $\alpha[1950] = 05^h32^m50^s.0$, $\delta[1950] = -05°25'36''.12$. The high velocity (HV) component appears at the left. The smooth line superposed upon the V spectrum represents a magnetic field of -60 μG. These spectra come from map data smoothed to a resolution of 40″.

ative of the I spectrum (both expressed in temperature units). The field can be computed on this basis for each channel individually, or else it can be computed across a range of channels by a least-squares fitting procedure. (See Troland and Heiles 1982*a*, and Schwarz *et al.* 1986 for further discussion of these techniques.) For present purposes we chose the least-squares approach because the sensitivity of the V spectra is insufficient to justify the channel-by-channel computation.

The fitting process for a pair of I and V spectra (at a given pixel) takes place in two steps. First the spectra are fitted over the full range of frequency channels to the function

$$V(f) = c_1 I(f)\,, \tag{1}$$

where c_1 is nonzero if the system gain is unequal in the two circular polarization senses. Typical values of c_1 in the present data are 0.01 to 0.02 or less. The difference $V(f) - c_1 I(f)$ is the V spectrum corrected for gain imbalance, that is $V^*(f)$. Next, the gain-corrected V spectrum is fitted to the function

$$V^*(f) = c_2\, dI/df\,, \tag{2}$$

where $c_2 = \frac{1}{2} zB$ and z has the value 2.8 Hz μG^{-1} for the 21 cm line. Typical values for the Zeeman splitting c_2 are 50 to 100 Hz. The fit to equation (2) yields an estimate of the line-of-sight field strength B and of the standard deviation $\sigma(B)$ of the field. In practice, we fitted each pair of I and V spectra twice to equation (2), choosing different ranges of channels to isolate the two velocity components in the profiles. To illustrate the results of the fitting process, we show as a dashed line in Figure 2 the dI/df spectrum scaled for a field of -60 μG. For this particular position, the derived fields in the two velocity components are not significantly different.

III. H I OPTICAL DEPTHS TOWARD ORION A

Lockhart and Goss (1978, hereafter L&G) describe the Orion A H I optical depth distribution observed at the Owens Valley Observatory at 2′ resolution. We have also computed optical depths from the present higher resolution data. In the discussion that follows, we emphasize features of the optical depth distribution pertinent to the discussion of magnetic fields in front of Orion A. A more detailed discussion of H I optical depths toward the source is presented by P. P. van der Werf, W. M. Goss, and D. S. Retallack (1989, in preparation) who have mapped the source with 18″ resolution.

The higher velocity (HV) H I component toward Orion A has a typical full width at half-power (FWHP) of between 2 and 3 km s^{-1} and a central velocity of 5.5 km s^{-1}, with the central velocity increasing toward the northeast. The lower velocity (LV) component has a typical FWHP of 3.5 to 5 km s^{-1} and a central velocity of 0 to 3 km s^{-1}, with values as low as -2 km s^{-1} in the extreme south of the source. The LV component also has a small velocity gradient directed to the northeast. L&G define a third "negative velocity" component that is strongest in the south of the source. We see this feature as well, but it does not appear to be truly distinct. Instead it appears to be the LV component which has a negative velocity at the extreme southern edge of the source.

Figure 3 represents the distribution of $\int T_{\rm H\,I}\, dv$ across Orion A at full (i.e., 25″) resolution. This figure includes both velocity components. Values for $\int \tau_{\rm H\,I}\, dv$ range from 12 to 30 km s^{-1}, with the highest values in the northeast quadrant of the source. Lowest values for $\int \tau_{\rm H\,I}\, dv$ occur in a small region near the southeast edge of the source and especially on the western edge. Some care must be taken in interpreting contours in the northeast quadrant of Figure 3. In this region the distribution of H I optical depths is quite uncertain owing to unmeasurably high optical depths (i.e., $\tau \geq 4$).

In order to more easily quantify the optical depth distribution in front of Orion A, we fitted Gaussians to the optical depth profiles across the source. Since the primary purpose of this study was to map the magnetic field distribution, and since sensitivity limitations in this endeavor ultimately forced us to smooth the spectral line data to a resolution of 40″, all discussion (and maps) that follow refer to data at that resolution. The optical depth profiles used in the fitting process are limited by sensitivity considerations to $\tau \leq 4$ and to regions in the map having $S_\nu \geq 2$ Jy per synthesized beam area.

In Figures 4 and 5 are maps of $\int \tau_{\rm H\,I}\, dv$ for the HV and for the LV component, respectively. Each value in these figures comes from the parameters of the Gaussian fits. At many positions in front of Orion A $\tau \gg 4$. These positions are represented in Figures 4 and 5 as filled circles. At a few positions the lines are only slightly saturated ($\tau \approx 4$). At these positions we have indicated lower limits for $\int \tau_{\rm H\,I}\, dv$. We estimate from a visual inspection of the optical depth profiles that the true values for $\int \tau_{\rm H\,I}\, dv$ at these positions are no more than 20% higher than the limits. Contour lines in Figures 4 and 5 are intended to give an indication of the optical depth distributions.

H I optical depths appear to be high for both velocity components in the northeast quadrant of the source. However, some confusion arises because the central velocity of the LV

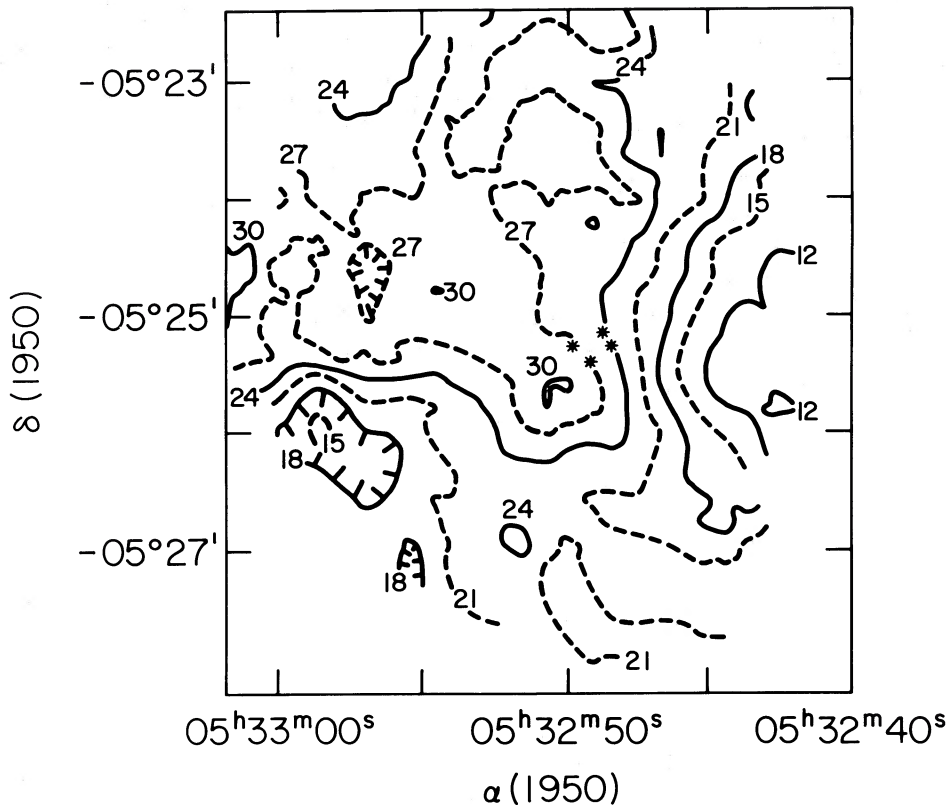

FIG. 3.—Map of the integrated H I optical depth $\int \tau_{HI} dv$ for all velocities in front of Orion A at full resolution (25″). The units are km s^{-1}. Asterisks in this figure (and in Figs. 4, 5, 6, 7, and 9) represent the Trapezium stars.

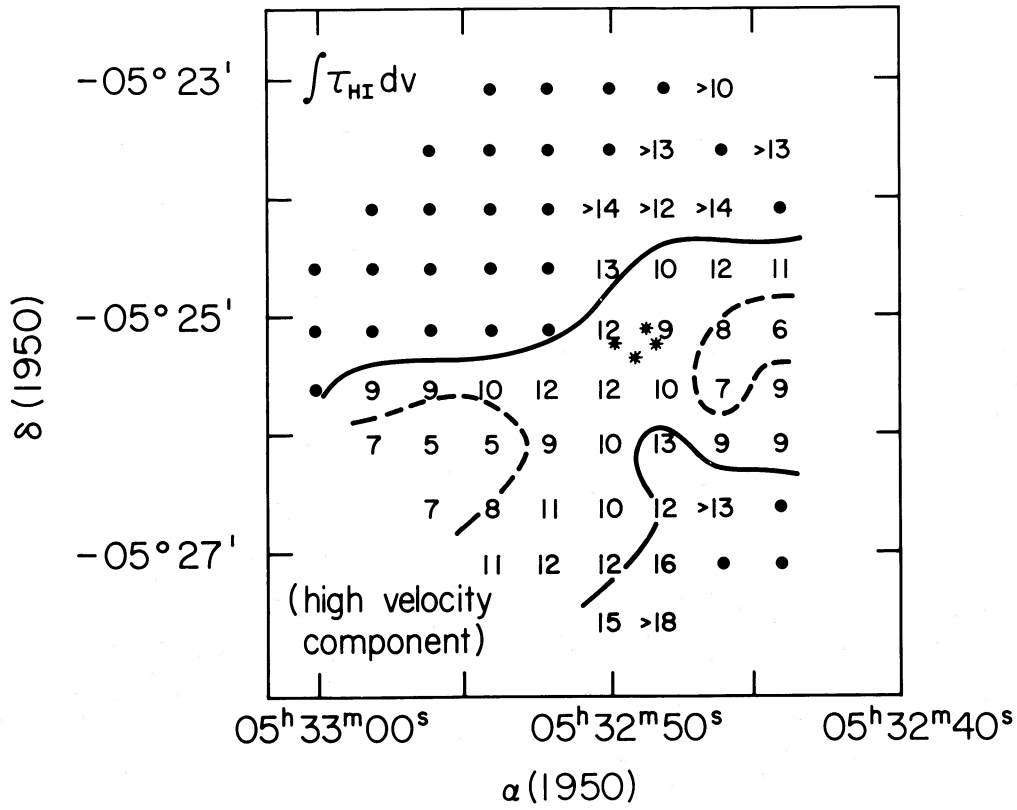

FIG. 4.—Map of $\int \tau_{HI} dv$ for the higher velocity (HV) H I absorption component in units of km s^{-1}. The spatial resolution of this map is 40″. Values have been computed from Gaussian fits to optical depth profiles. The solid lines denote regions for which $\int \tau_{HI} dv \geq 13$ km s^{-1}, while the dashed lines represent regions for which $\int \tau_{HI} dv \leq 8$ km s^{-1}. Filled dots represent positions at which the profiles are highly saturated (i.e., $\tau \geq 4$). Lower limits at several positions are estimated to be within 20% of the true values (see text).

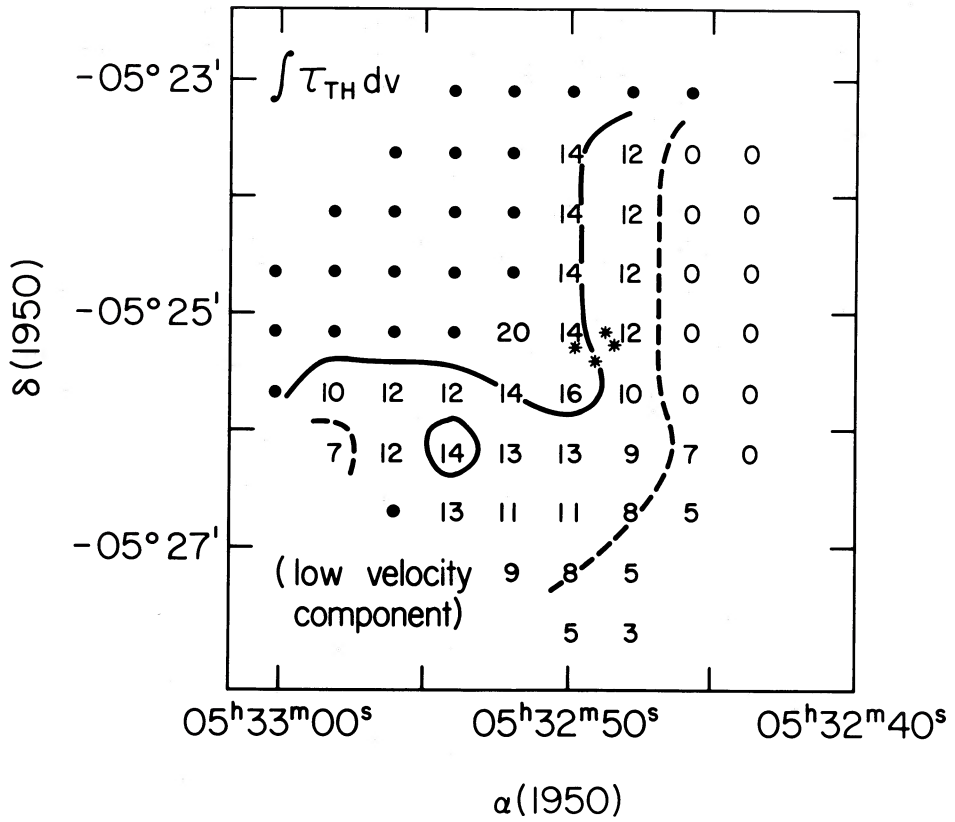

FIG. 5.—The same as Fig. 4 for the lower velocity (LV) component. Solid lines denote regions for which $\int \tau_{H\,I}\, dv \geq 14$ km s^{-1}, while the dashed lines denote regions having $\int \tau_{H\,I}\, dv \leq 7$ km s^{-1}.

component is highest here ($v_0 \approx 4$ km s^{-1}), and the two components are more blended than elsewhere across the source. Therefore, it is impossible to determine unambiguously if only one component has high optical depth (most probably the HV one) or if they both do. The northeast quadrant is the same region where the "dark lane" of optical extinction separates Orion A from NGC 1982 and where the "dark bay" of extinction protrudes westward across Orion A. Owing to sensitivity limitations in our data, it is impossible to tell if the very brightest H I optical depths really coincide with this latter optical feature. However, for both velocity components, the southern boundary of the dark bay coincides with the southern boundary of the H I region that is saturated in our data. (See the [S II] λ6717–6731 Å image reproduced in Fig. 13 of L&G.)

Outside the northeast quadrant of the source, the overall distributions of integrated optical depths are quite different for the two components. For the HV component, $\int \tau_{H\,I}\, dv$ is highest (and mostly saturated) throughout the northern half of the source and at the southwestern edge. This latter region of high optical depth nearly coincides with a small dark patch of optical extinction. For the LV component, $\int \tau_{H\,I}\, dv$ increases almost monotonically from southwest to northeast. For both components, $\int \tau_{H\,I}\, dv$ is relatively low at the western edge of the source. This is especially true for the LV component which is undetected along most of the western edge of the source. The distributions of $\int \tau_{H\,I}\, dv$ from the present data are quite consistent with the lower resolution maps of L&G.

In the unsaturated regions of the maps $\int \tau_{H\,I}\, dv$ is typically 8 to 15 km s^{-1} for either velocity component, therefore $N_{H\,I}/T_{ex}$ is in the range 1.5 to 3 × 10^{19} cm^{-2} K. If $T_{ex} \approx 29$ K (§ VII*b*), then the H I column densities for each of the components are in the range 4 to 8 × 10^{20} cm^{-2}. Thus, each component contributes about the same column density, assuming the same T_{ex}. If $N_p/E(B-V) = 5.8 \times 10^{21}$ cm^{-2} mag^{-1} (Bohlin, Savage, and Drake 1978), where $N_p = H_{H\,I} = 2N_{H_2}$, and if the ratio R of total to selective extinction toward Orion A is 3.1, then each velocity component contributes between 0.2 and 0.4 mag of visual extinction. Column densities and extinctions in the saturated regions ($\tau \geq 4$) of the maps could easily be a factor of 2 or more higher, with extinctions possibly much higher if H_2 is present.

IV. THE DISTRIBUTION OF MAGNETIC FIELD STRENGTHS

In Figures 6 and 7 we present maps of the line-of-sight magnetic field strengths for the HV and for the LV components, respectively. All values in these two figures are truly negative (field pointed toward the observer) with the exception of one in Figure 7 denoted by a plus sign. We are doubtful about the significance of this point. In all subsequent discussions, the sign of the field will be ignored.

Care is needed in interpreting Figures 6 and 7 because the significance of the fitted field strengths [i.e., $B/\sigma(B)$] varies considerably with position. For both velocity components, $B/\sigma(B)$ is as high as seven at some positions where the continuum brightness is high and the line is also narrow. In order to convey the essence of this information in the figures, we have plotted in large type those field values for which $B/\sigma(B) \geq 3$. These values are quite reliable. Field values for which $2 \leq B/\sigma(B) < 3$ are shown in smaller type to indicate their lesser significance. Finally, we have shown in parentheses a very few

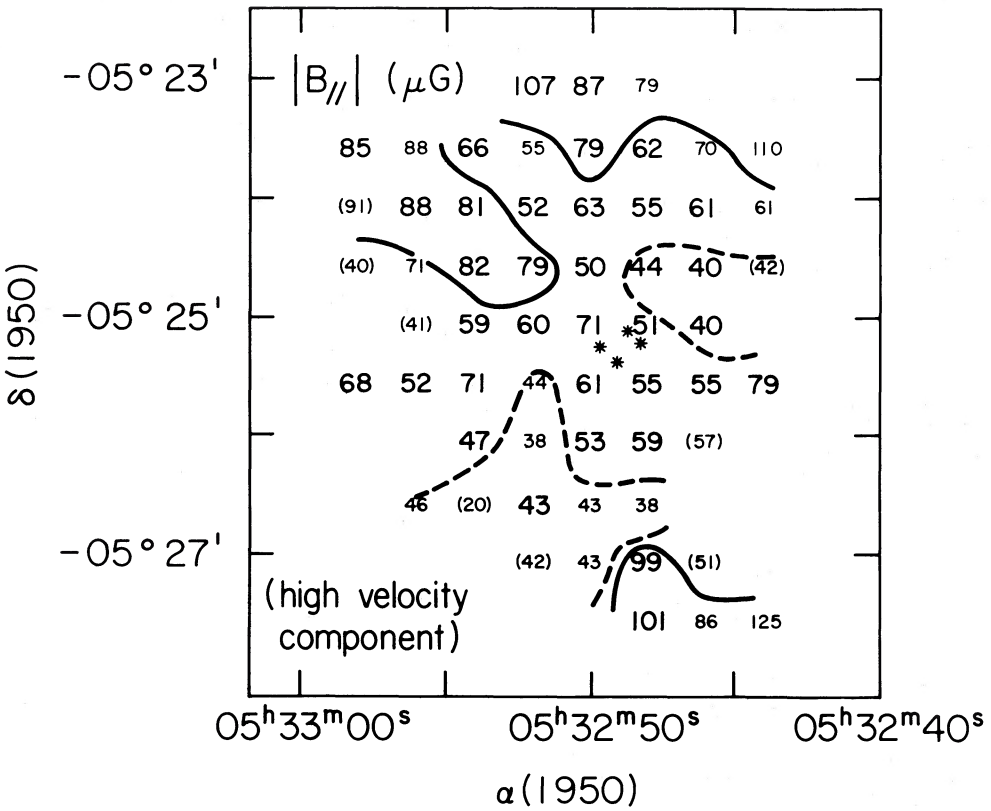

FIG. 6.—Map of the line-of-sight magnetic field strength in the HV component at a spatial resolution of 40″. Absolute values are shown, all values are negative. Values in large type are those for which $|B|/\sigma(B) \geq 3$. Values in small type are those for which $2 \leq |B|/\sigma(B) \leq 3$. Values in parentheses are those for which $1 \leq |B|/\sigma(B) \leq 2$. The solid line denotes those regions having $|B| \geq 75$ μG, the dotted line denotes those regions having $|B| \leq 50$ μG.

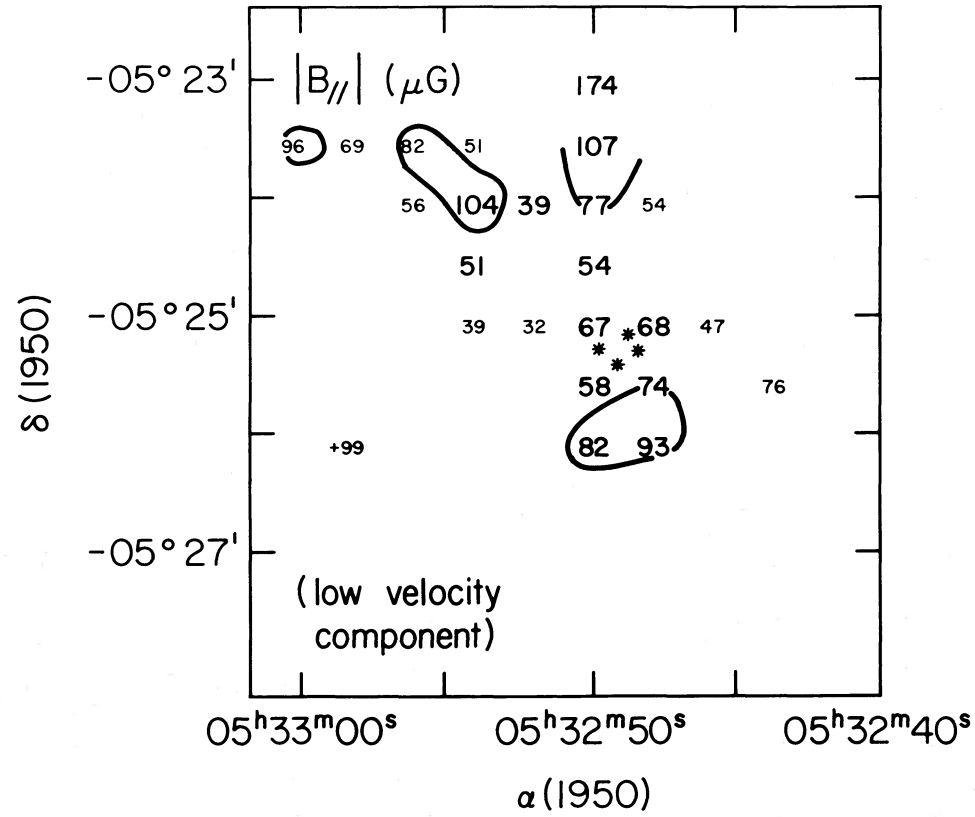

FIG. 7. The same as Fig. 6 for the LV component

field values for which $1 \leq B/\sigma(B) < 2$. Although the significance of these results is quite low, they may convey some useful information especially when they are comparable to other higher significance values at adjacent positions.

In the HV component (Fig. 6), reliably detected values of B_{HV} range from about 40 ± 13 μG to a little over 100 ± 25 μG, with most values in between 40 and 80 μG. It is noteworthy that the direction of the field does not reverse at any position in front of the source, any more than it does in the H I regions in front of Cas A (Schwarz *et al.* 1986). In general, the higher values of B_{HV} (≥ 60 μG) lie in the north and northeast sector of the source and in a small region at the southwest edge. The very highest values [≥ 80 μG, with $\sigma(B)$ typically 20 μG] occur along the northern rim of the source, in a "tongue" extending from the northeast edge inward toward the center, and at the southwest edge. The lowest values of B_{HV} (≤ 50 μG) are concentrated in the southeastern and also in the west central part of the source.

Since the LV component is wider than the HV component, sensitivity to magnetic fields is less. (The expected error in deriving the field from Zeeman effect data is proportional to the square root of the line width.) Therefore, the magnetic field map for the LV component (Fig. 7) contains many fewer points than the map for the HV component, and the general distribution of B_{LV} is difficult to judge. Field strengths run from about 40 ± 15 μG to well over 100 ± 20 μG, with several of the positions having $B_{LV} \geq 100$ μG and $B_{LV}/\sigma(B) \geq 6$.

In Figure 7 (LV component), two prominent regions of high field stand out. One is in the northern and northeastern region of the source; the other is just southwest of the map center. In the former region the field is exceptionally strong. The highest value is 174 ± 45 μG, comparable to the 125 ± 20 μG reported by Troland, Crutcher, and Kazès (1986) for the OH absorbing region in front of Orion A. Owing to the uniqueness of this H I result, we present the *I* and *V* spectra in Figure 8. High field values also exist in the HV component (Fig. 6) near this position. The other high field region in the LV component (i.e., southwest of map center) has a sharp discontinuity in field strength at its southern edge. The field drops from between 80 and 90 ± 12 μG to an undetectable 20 ± 20 μG in the adjacent pixels. There is also a sharp discontinuity in B_{LV} in the high field region at the north of the source.

The magnetic field distributions for the two velocity components appear to be similar. This similarity is likely to be significant, and it bears upon the physical nature of the two H I regions (§ VII*a*). Nonetheless, some differences do exist. To identify such differences, we computed for each map point the quantity $\Delta B = B_{HV} - B_{LV}$ and also the error in this difference $\sigma(\Delta B)$. There are several regions in the map where $\Delta B \geq 2\sigma(\Delta B)$ for two or three adjacent pixels. In one such region, to the southwest of map center, $B_{LV} > B_{HV}$. In two other regions $B_{HV} > B_{LV}$; one is at the southwestern edge of the map, the other is in the northeast part of the map at the end of the tongue of high B_{HV}.

V. A COMPARISON OF MAGNETIC FIELD AND H I OPTICAL DEPTH DISTRIBUTIONS

A major goal of the present study is to search for a correlation between the distribution of magnetic field strengths and gas column densities. If such a correlation is found, it many indicate a relation between gas *volume* density and field strength. Indeed, such a relation seems to exist in the H I gas toward Cas A (Schwarz *et al.* 1986). Also, a direct comparison between field strengths and gas column densities can serve as an indication of the mass-to-flux ratio in interstellar clouds. The mass-to-flux ratio characterizes the manner in which mass is loaded onto tubes of magnetic flux in the clouds (Mouschovias 1967*a*, *b*). This ratio may vary with position in a cloud, and it does not change (in comoving coordinates) as a cloud expands or contracts with a frozen-in magnetic field. Variations in the mass-to-flux ratio within interstellar clouds may have a significant influence upon cloud evolution. No theory exists to predict such variations—they must be determined observationally.

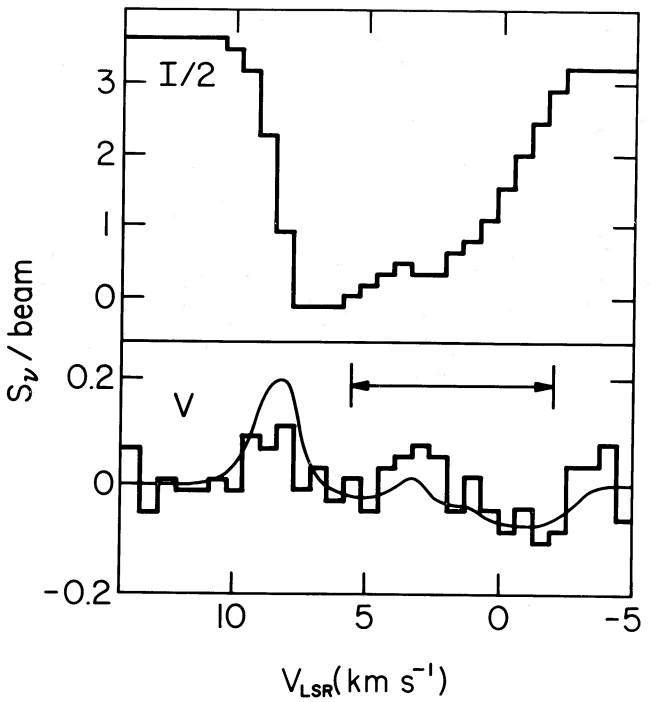

FIG. 8.—The same as Fig. 2 except for the position $\alpha[1950] = 05^h32^m50^s.0$, $\delta[1950] = -50°23'06''.12$. The smooth line superposed upon the *V* spectrum represents a magnetic field of -174 μG, fitted over the channels denoted by the horizontal arrow.

For the HV component, the distribution of *B* (Fig. 6) is qualitatively similar to the distribution of $\int \tau_{H\,I}\,dv$ (Fig. 4). High field regions (i.e., $B_{HV} \geq 75$ μG) in the north and northeast of the source lie within regions where the H I optical depth profiles are saturated in our maps at $\tau \geq 4$. The high field region at the southern edge of the source appears to be closely associated with the region of high $\int \tau_{H\,I}\,dv$ in the south and southwest. The two regions of relatively low field (i.e., $B_{HV} \leq 50$ μG) in the southeast and west of the source appear to correspond with (but to be slightly displaced from) similar regions of low $\int \tau_{H\,I}\,dv$.

This qualitative correspondence between B_{HV} and $\int \tau_{H\,I}\,dv$ suggests that variations in B_{HV} principally reflect variations in *total field strength* rather than direction of the field lines. Heiles (1988) has argued that a correlation between the line-of-sight field strength and the radial velocity of the line may indicate the opposite circumstance, that is, variations in line-of-sight field strength arising primarily from variations in field direction. No such correlation between B_{HV} and the radial velocity of this component is apparent, consistent with the interpretation that the map of B_{HV} (Fig. 6) is representative largely of variations in total field strength.

Despite the qualitative correlation that exists between field strengths and H I optical depths in the HV component, no clearly defined *quantitative* connections is apparent if the two are plotted against each other. This circumstance may result in part from statistical errors in the individual field strength measurements. It may also reflect the tendency of corresponding morphological features in Figures 4 and 6 to be slightly displaced from each other in the sky (see above). Such displacements, in turn, may be a residual effect of field curvature upon the line-of-sight field strengths. A more complete comparison between B and $\int \tau_{\rm H\,I}\,dv$ could be made if the H I line were not saturated in the northeast part of the source.

In the LV component no correlation between B and $\int \tau_{\rm H\,I}\,dv$ is apparent, probably because the sensitivity is reduced. The high $B_{\rm LV}$ regions in the northeast lie mostly within the heavily saturated region of the map. The other high B region to the southwest of the map center does not correspond with an isolated region of high $\int \tau_{\rm H\,I}\,dv$, but it does lie at the tip of the high $\int \tau_{\rm H\,I}\,dv$ region which extends from the northeastern sector of the source.

VI. OPTICAL EXTINCTION ACROSS ORION A

In comparing magnetic field structure with the distribution of gas in front of Orion A, the distribution of optical extinction (A_v) can provide an important additional source of information. A_v is measurable even at positions where the H I maps are saturated, and A_v is not sensitive to $T_{\rm ex}$ as is the H I optical depth. Also, A_v is sensitive to total gas column density including the molecular gas in front of the nebula for which no high-resolution radio frequency maps exist. A complicating factor is that optical extinction can occur in the H II gas as well as in the foreground neutral gas.

a) Determination of A_v From Previously Published Data

We estimated A_v over Orion A using the standard technique employed by Chaisson and Dopita (1977). In this technique, the distribution of Hβ flux (F_β) is compared with the radio frequency brightness distribution at a frequency high enough for radio continuum optical depths to be low. The radio brightness is proportional to I_β, the intrinsic (i.e., unobscured) Hβ flux from Orion A. For the radio brightness distribution, we chose the single-dish 23 GHz map of Wilson and Pauls (1984) with a spatial resolution of 42″. Existing *synthesis* maps of the Orion A radio continuum are not optimum for this purpose. Either they are missing flux density (the 6 cm map of Johnston *et al.* [1983] contains only 22.5% of the total [Wilson and Pauls 1984]), or else they are at too low a frequency to ensure small optical depths at all map positions (e.g., Fig. 1). For the F_β distribution we used the calibrated isophotal map of Dopita, Isobe, and Meaburn (1975). This map has an effective spatial resolution of about 15″.

To estimate the optical extinction across Orion A, we first smoothed the F_β map of Chaisson and Dopita to a resolution of about 35″, comparable to that of the radio continuum map and to the magnetic field maps. Next we applied the same relation used by Chaisson and Dopita to compute I_β from the radio brightness. The ratio F_β/I_β (ranging from 0.4 down to 0.04) is related to the dust optical depth τ_β in a way that depends upon the location of the dust. If the dust lies entirely *in front of* the H II region, the $F_\beta/I_\beta = e^{-\tau_\beta}$ and $\tau_\beta \approx 0.9$ to 3.2 across the source. If the dust is entirely *within* (and well mixed with) the H II gas, then $F_\beta/I_\beta = (1 - e^{-\tau_\beta})/\tau_\beta$ and $\tau_\beta \approx 2.2$ to 25. In either case $A_v \approx \tau_\beta$ to within a few percent.

b) Location of the Obscuring Dust

In Figure 9 we present the distribution of A_v across Orion A, assuming that the obscuring dust lies entirely *in front of* the H II region [i.e., $A_v \approx \tau_\beta = -\ln (F_\beta/I_\beta)$]. This assumption cannot be completely correct as discussed below; however, even if it is not correct, the morphology of the extinction distribution in Figure 9 is still reliable although the values for A_v are too low.

Simple estimates suggest that the extinction within the H II region should be quite high. Models for Orion A have $N_p \geq 10^{22}$ cm^{-2} through the center (Lockman and Brown 1975; Shaver 1980). Thus $A_v \geq 9.5$ mag in the ionized gas, given the values of R and $N_p/E(B-V)$ cited above. Yet $F_\beta/I_\beta = 0.22$ at the radio continuum peak. This value implies $A_v \leq 4.5$ mag in the H II region. Evidently, the actual extinction toward the center of the H II region (inferred from F_β/I_β) is substantially less than expected from the column density and gas-to-dust ratio. This inconsistency, if not a result of systematic errors in F_β/I_β, may arise from an underabundance of dust in the ionized gas. The spectrophotometric studies of O'Dell and Hubbard (1965) indicate that the dust-to-gas ratio is at least an order of magnitude smaller in the inner regions of the Orion Nebula relative to the outer regions.

Independent of other considerations, there is good reason to believe that much of the extinction toward the Orion Nebula does arise in the neutral forground gas, as assumed in Figure 9. The morphology of the A_v map does *not* mimic that of the radio brightness distribution, contrary to the conclusions drawn by Martin and Gull (1976). Instead, the morphology of A_v resembles the distribution of $\int \tau_{\rm H\,I}\,dv$. A_v is highest in the northeast quadrant of the source in the direction of the dark bay where the H I map is saturated. A second peak in A_v to the south and southwest coincides quite closely with the H I optical depth peak in the HV component and with a small patch of extinction clearly visible on optical images of the nebula. The regions of lowest A_v in the west central and in the southeastern portions of the source are regions of low $\int \tau_{\rm H\,I}\,dv$ as well. This qualitative correlation between A_v and $\int \tau_{\rm H\,I}\,dv$ suggests that in the regions of unsaturated H I, no significant concentrations of H_2 are likely to exist having scale sizes of order 40″ or more, otherwise they should make a recognizable contribution to A_v. Evidently, the minima in $\int \tau_{\rm H\,I}\,dv$ represent true minima in neutral gas column densities, not regions where H_2 exists in place of H I nor regions of warmer H I.

As a quantitative test of the correlation between A_v and $\int \tau_{\rm H\,I}\,dv$, we have plotted these two parameters against each other in Figure 10. In the figure $\int \tau_{\rm H\,I}\,dv$ is the sum of the values for the HV and LV components (Figs. 4 and 5). Pixels for which $\int \tau_{\rm H\,I}\,dv$ is saturated in either component (i.e., pixels represented as filled dots in Figs. 4 and 5) and pixels for which only an upper limit exists for either component have been excluded in Figure 10. A linear relationship clearly exists between A_v and $\int \tau_{\rm H\,I}\,dv$. A least-squares fit to the 32 points yields the relation $A_v = 0.89 + 0.034 \times \int \tau_{\rm H\,I}\,dv$ mag (shown as a dashed line in Fig. 10). This result suggests that about one magnitude of large angular scale extinction exists along the line of sight to Orion A (and possibly within the H II region itself), and that the remainder of the extinction arises within the small angular scale H I gas directly in front of the nebula. The slope of the linear fit to the points of Figure 10 is proportional to the product $RT_{\rm ex}$, given the standard value for $N_p/E(B-V)$ and assuming that the extinction arises entirely within atomic gas. If $T_{\rm ex} = 29$ K (§ VII*b*, below), then the slope of the fit

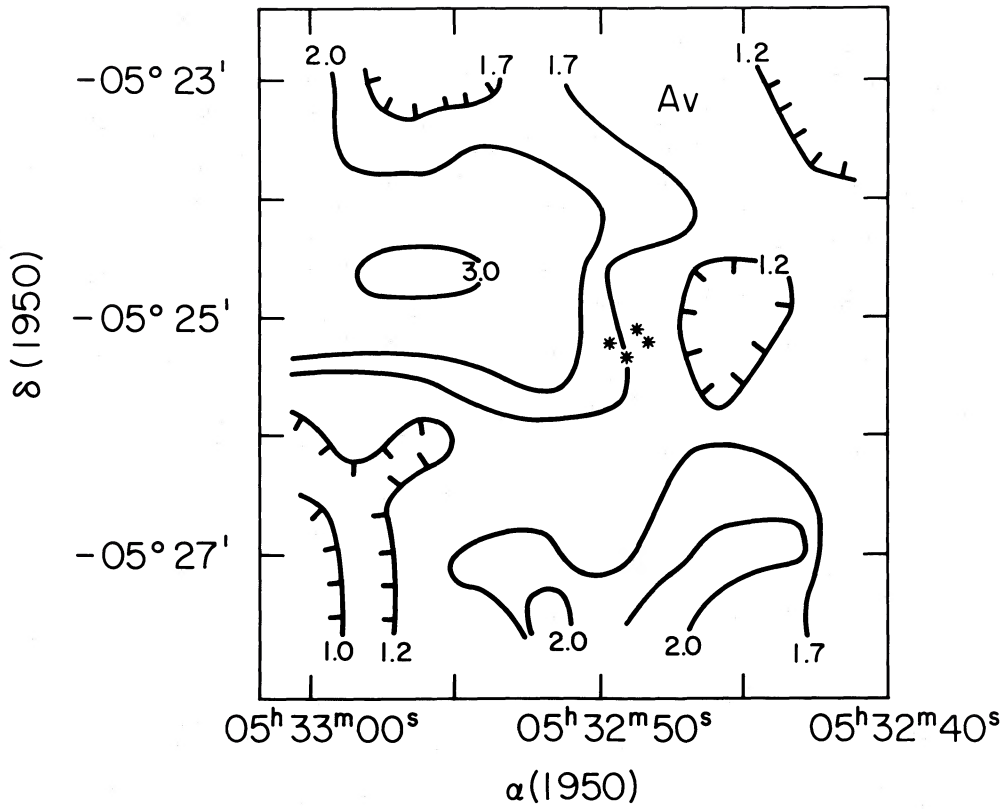

FIG. 9.—Map of A_v in front of Orion A based upon radio and optical data (see text). The spatial resolution is 40″.

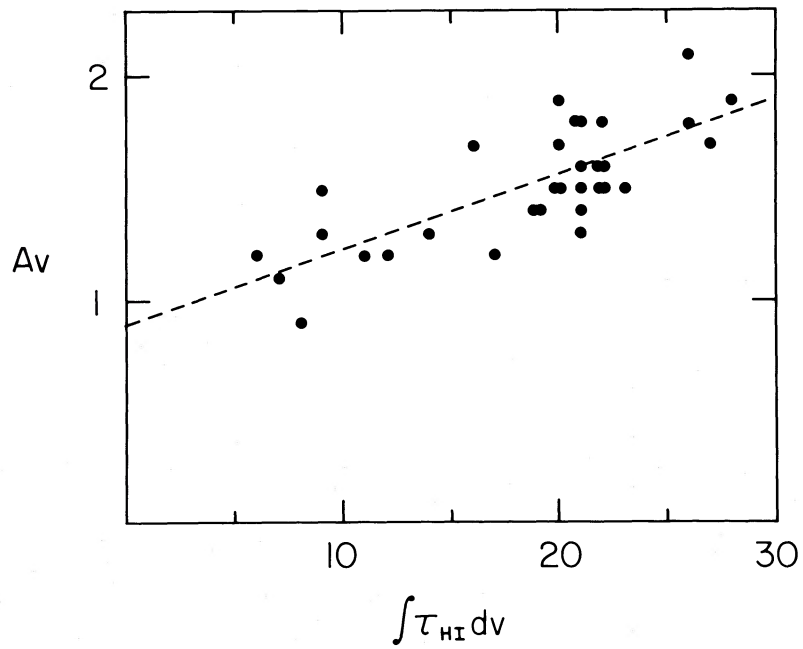

FIG. 10.—A plot of A_v as a function of $\int \tau_{\rm H\,I}\,dv$ for both H I velocity components combined. Positions for which only upper limits to $\int \tau_{\rm H\,I}\,dv$ are known have been omitted from this plot. The dashed line is a least-squares fit to the data points.

implies $R = 3.7$ in the small angular scale H I gas in front of Orion A. This value lies between the standard interstellar value of 3.1 and the higher value of 5.5 proposed by Lee (1969) for extinction within the H II region itself. Since the value of T_{ex} is somewhat uncertain and may not be uniform, the ratio R derived from the slope in Figure 10 cannot be used to discriminate reliably between these two limits.

Chaisson and Dopita (1977) also present a map of A_v across the face of Orion A. This map is generally similar to the map in Figure 9. The highest extinctions in both maps arise in the dark bay, and extinctions are low to the southeast of the bay. However, the two maps differ in many details. These differences arise in part because of the lower resolution of the Chaisson and Dopita map (1.'3 versus 40″). The differences probably also arise because of instrumental effects in their continuum map, effects which are apparent in comparing their map with that of Wilson and Pauls (1984).

c) *The Magnetic Field Distribution and A_v*

Only B_{HV} can be meaningfully compared to the distribution of A_v across Orion A since B_{LV} is not well determined at many positions. Over most of the source, the qualitative correlation between B_{HV} and A_v is reasonably good. The tongue of high B_{HV} in the northeast lies within the region of high A_v associated with the dark lane, but it is displaced as much as 30″ north of the region of highest A_v. The peak in B_{HV} at the southwest edge of the source lies within a region of enhanced A_v. Also, the regions of low B_{HV} in the southeastern and in the west central zones of the source seem to correspond with regions of lower A_v. However, the regions of high B_{HV} in the extreme north and northwest edges of the source have no corresponding structure in the A_v map. The qualitative correspondence between B_{HV} and A_v lends weight to the conclusion of § V that variations in B_{HV} largely reflect variations in actual field strength rather than changes in field curvature.

VII. THE NATURE OF THE FOREGROUND GAS AND FIELD

The physical nature of the neutral gas lying in front of the Orion Nebula is less well known than that of the more massive and more intensively studied molecular cloud behind. Indications of the presence of this gas, apart from the H I absorption and optically obscured features discussed above, include UV H I absorption (Savage and Jenkins 1972), 18 cm OH absorption (Goss 1968; Troland *et al.*), 6 cm H_2CO absorption (Zuckerman, Palmer, and Rickard 1975) and low-frequency C II lines that have been attributed to stimulated emission in the foreground gas (Ahmad 1976; Jaffee and Pankonin 1978).

a) *Location of the Foreground Gas and Field*

Most of the H I absorbing gas along the line of sight to Orion A almost certainly lies close to the ionized gas. Several lines of evidence support this inference. For example, L&G have noted the similarity in velocity gradients between H I and H II gas. Also, the H I absorption profiles are characterized by just two components, both of which exhibit a clear rise in optical depth toward the northeast in the direction of the dark lane and dark bay. These latter features, in turn, have long been recognized as a part of the larger molecular cloud from which the nebula and Trapezium stars formed. An indication of the close association between the dark bay and the H II region is the notch in the continuum emission (Fig. 1) that coincides with the western edge of the dark bay. This feature was previously noted by Martin and Gull (1976); it appears most clearly in the 21 cm continuum map of P. P. van der Werf, W. M. Goss, and D. S. Retallack (1989, in preparation).

Further evidence for a connection between the H I gas and the Orion Nebula region comes from the similarities in central velocities and widths of the H I HV component, the C II lines, and the molecular lines arising in front of the nebula. The Orion A C II lines have two velocity components, at 9 km s^{-1} and at 6 km s^{-1} (e.g., Ahmad 1976 and references therein). The lower velocity component is attributed to stimulated emission in the neutral foreground gas (Zuckerman and Ball 1974; Ahmad 1976; Jaffee and Pankonin 1978), and its central velocity and width (as measured by Jaffee and Pankonin) match quite closely those of the H I HV component. Given the analysis of Walmsley (1975), C II should permeate the H I gas in front of the H II region.

The existence of molecular gas in front of Orion A is established by the presence of weak 6 cm H_2CO and 18 cm OH absorption lines. The former were observed by Zuckerman *et al.* at selected positions with the Bonn telescope (half-power beam width 2.'6). OH lines have been observed at high sensitivity as a part of the OH Zeeman observations of Troland *et al.* This work was performed with the Nançay telescope having a half-power beam width in α and δ of 3.'5 and 18′, respectively. Because of the limited angular resolution of the OH and H_2CO data, little information exists about the spatial distribution of these lines; however, central velocities and half widths are very close to those of the H I HV component. Most probably, the molecular gas is largely confined to the dark bay and dark lane in front of the source, a view supported by the absence of detectable UV H_2 absorption lines toward Θ^1 Ori (Savage *et al.* 1977). Unfortunately, none of the H_2CO positions of Zuckerman *et al.* overlaps the dark bay or dark lane.

The body of available evidence suggests a configuration for the gas in front of Orion A as follows: the H I HV component lies closest to the H II region since its velocity matches that of the C II lines which arise nearest the H I–H II interface. In addition, the small-scale structure in $\int \tau_{HI}\, dv$ for the HV component (Fig. 4) largely matches that of A_v (Fig. 9). This coincidence may arise if much of the small-scale structure in the neutral gas exists in the regions closest to the H II region rather than in more diffuse outlying regions. Farther away from the H II region, but still physically associated with the H I HV gas, the molecular gas is confined mostly to the dark bay and lane. The H I LV component at $v \approx 0$ to 3 km s^{-1} is even more distant from the H II region. It shows less spatial structure in $\int \tau_{HI}\, dv$ and it may well form a more diffuse envelope around the near side of the Orion region.

All three regions (i.e., the two H I velocity components and the H_2) are threaded by a common magnetic field. The common nature of this field, at least for the H I components, is suggested by the similarities that exist in the measured strengths (Figs. 6 and 7). The field points toward the observer and may lie nearly parallel to the line of sight. (If not, the actual field strengths are considerably higher than those measured.) An orientation of the field along the line of sight is also consistent with the observed absence of significant optical polarization of the Trapezium stars (Breger 1976). This absence exists despite indications that much of the visual extinction toward the H II region arises in the foreground neutral material (§ VI*b*) and despite the fact that this foreground material is permeated by a strong and probably well-ordered magnetic field (§ VII*c* below).

Spatial structure observed in B_{HV} primarily reflects varia-

tions in total field strength rather than in field direction because regions of high B_{HV} correspond to regions of proportionately higher $\int \tau_{HI} dv$ (§§ V, VIc). This correspondence, in turn, suggests that the field is distributed such that the mass-to-flux ratio is roughly constant, and that the field strength increases with volume density of the gas. This latter suggestion is consistent with the theoretical expectation that field strengths and gas densities should be related under many circumstances. It is also consistent with the growing body of observational evidence that the field strength indeed does tend to increase with volume density, for large enough densities. Other evidence for this field strength-volume density connection is discussed by Troland and Heiles (1986), by Heiles (1987*a*, *b*), by Schwarz *et al.* (1986) for the H I clouds in front of Cas A, and by Crutcher *et al.* (1987) for molecular clouds.

b) H I *Temperatures and Densities*

Following the procedure of L&G, we estimated the H I excitation temperature in front of the H II region from the observed values of N_{HI}/T_{ex} toward Θ^1 and Θ^2 Ori (average value 3.8×10^{19} cm^{-2} K^{-1}) and from the value of N_{HI} derived for the two stars in the UV (1.1×10^{21} cm^{-2}, Savage and Jenkins 1972). From this information $T_{ex} \approx 29$ K, close to the result of 25 K proposed by L&G. This estimate, of course, is based on the assumption that the average gas column density measured over the the 40″ synthesized beamwidth is the same as that along the lines of sight to the stars. Some additional support for a temperature in the range 20–30 K may come from the low-frequency C II lines observed toward the H II region. Ahmad (1976) modeled these lines, and he found that a satisfactory fit for the 6 km s^{-1} lines arising in the foreground gas could be achieved only for $T_e \approx 20$ K. However, several other authors who attempted to derive T_e in this C II region concluded that the results are largely indeterminate (e.g., Jaffee and Pankonin 1978; Boughton 1978) or that T_e varies strongly with dust optical depth (Qaiyum and Razullah Ansari 1983).

Densities in the H I gas have been estimated by L&G to be of the order of a few times 10^2 cm^{-3}. The present data are consistent with these values. For example, in the HV component N_{HI} is typically about 6×10^{20} cm^{-2} if $T_{ex} = 29$ K. Variations in N_{HI} in the HV component occur over angular scales of 3′, or 0.4 pc at a distance of 500 pc. If this same length scale applies along the line of sight, then $n_{HI} \approx 400$ cm^{-3}. This density is comparable to densities in the H I clumps along the line of sight to Cas A where magnetic field strengths are similar to those reported here (Schwarz *et al.* 1986). In the molecular gas responsible for the OH absorption, Troland *et al.* estimate $n(H_2) \approx 10^4$ cm^{-3}. Actual densities in the H I gas toward Orion A could be considerably higher than estimated above since the H I profiles are heavily saturated at many positions (§ III).

c) *Dynamical Importance of the Magnetic Field*

The dynamical importance of the magnetic field in the neutral foreground gas can be roughly estimated by application of the virial theorem. For this purpose, we assume the neutral gas in front of Orion A occupies a cylinder with its axis along the line of sight. The cylinder is assumed to have a constant hydrogen column density across its face of $N_p = 2.5 \times 10^{21}$ cm^{-2}, a value that reflects the average $A_v \approx 2$ mag across Orion A (Fig. 9). By using A_v to estimate N_p, we include molecular as well as atomic gas. The length (l) of the cylinder along the line of sight is N_p/n_p, which for $n_p \approx 400$ cm^{-3} implies $l \approx 2$ pc. Given a cylinder radius $r \approx 0.5$ pc, a kinetic temperature of 25 K, a velocity width for macroscopic motions of 3.5 km s^{-1} (from the H I line widths), and a field strength of 70 μG, we can estimate the mass of the region (22 $M_\odot$ including He) and the approximate values of the various virial terms. These values are given in Table 2.

TABLE 2

VIRIAL TERMS FOR THE NEUTRAL GAS IN FRONT OF ORION A

Term	Energy (10^{44} ergs)
Thermal	1.7
Macroscopic motions	55
Magnetic	200
Gravitational	0.8

It appears from Table 2 that the magnetic field has a very significant influence upon the neutral gas in front of Orion A. Only the virial term associated with macroscopic internal motions in the gas is comparable to that for the magnetic field; terms associated with thermal kinetic energy and gravitational energy are about two orders of magnitude smaller. Evidently, the dynamics in this region are controlled by the magnetic field and by the macroscopic velocity field. Of these two, the magnetic field may dominate especially since measured field strengths exceed 70 μG at a number of positions (Figs. 6 and 7). In view of these circumstances, the field is unlikely to be significantly tangled. Schwarz *et al.* (1986) drew similar conclusions for H I concentrations along the line of sight to Cas A.

Various uncertainties affect the computed values of the virial terms in Table 2. However, none is likely to influence the results by as much as an order of magnitude except uncertainties in the cylinder radius r. This parameter is largely unknown, since the neutral gas in front of Orion A may extend beyond the boundaries of the continuum source in the plane of the sky. In the model we have chosen, all virial terms scale as r^2 except for the gravitational term which scales approximately as r^3. Thus, the relative importance of the gravitational term is proportional only to r, and the conclusions stated above should be valid unless the neutral gas extends very far beyond the confines of Orion A.

VIII. THE ORION MAGNETIC ENVIRONMENT

The small-scale magnetic field in front of Orion A is presumably part of a much larger scale field revealed by a variety of observations. Evidence for the large-scale field comes in part from optical polarization studies. Appenzeller's (1974) study covered a 15° × 15° area centered on Barnard's Loop. His results show that over a length scale of 10 to 15° the field tends to be perpendicular to the Galactic plane, hence perpendicular to the long axis of the Orion A molecular cloud (see e.g., Maddalena *et al.* 1986). This same orientation is also evident in the all-sky optical polarization maps of Mathewson and Ford (1970). In these maps, polarization vectors also lie predominantly perpendicular to the Galactic plane in the region $l \approx 200°$ to 215°, $b \approx -10°$ to $-25°$; whereas in the same longitude range, the vectors for stars within 5° of the Galactic plane are parallel to the Galactic plane as usual. Most stars exhibiting such polarization perpendicular to the Galactic plane are at distances of 200 and 1000 pc. Evidently, the perpendicular geometry of the magnetic field in this direction persists over an appreciable distance along the line of sight.

Further evidence for large-scale magnetic field structures

comes from studies of Faraday rotation of extragalactic radio sources and from H I Zeeman effect. Faraday rotation does not arise in the neutral atomic or molecular gas owing to the scarcity of thermal electrons. Nonetheless, in the all-sky rotation measure map of Simard-Normandin and Kronberg (1980), the Barnard's Loop–Orion region is within a zone of positive rotation measures some 50° in diameter and centered near $l \approx 255°$, $b \approx -10°$. Positive rotation measures correspond to magnetic fields pointing *toward* the observer, the same field direction implied by the H I and OH Zeeman effect observations in the direction of Orion A. This same field direction is also implied by most of the (36′ resolution) H I Zeeman effect observations made by Heiles (1987*a*, *b*) at some 50 positions within the extended H I region surrounding the Orion A molecular cloud. Heiles (1987*a*, *b*) argues that those few positions where the field points *away from* the observer lie outside what may be a large (15° diameter) broken shell of molecular gas traced out in part by the Orion A cloud, the Orion B cloud, and the Mon R2 cloud of Maddalena *et al.* (1986). The field Heiles detects in these directions (i.e., outside the shell) may be located elsewhere along the line of sight and be unrelated to the H I/H_2 regions of Orion. However, there is at least one positive magnetic field within this candidate shell, the field of $+38$ μG in the OH absorbing region in front of Orion B (Crutcher and Kazès 1983; Heiles and Stevens 1986).

All available data suggest that a large-scale feature in the Galactic magnetic field permeates the Orion complex of atomic and molecular gas. The scale size of this feature is at least 15° or 130° pc at a distance of 500 pc. Within this feature, the field is oriented largely perpendicular to the Galactic plane, and it points in the direction of the observer. Typical field strengths in the H I emission regions are not high, 10 μG or less. The existence of this magnetic structure may be related to the formation process of the ccmplex itself, perhaps via the magnetic Raleigh-Taylor instability (e.g., Parker 1966; Mouschovias, Shu, and Woodward 1974). Alternatively, the magnetic structure may be a product of the complex itself, as once uniform field lines were driven outward by expansion of a stellar wind or supernova-blown shell.

IX. THE IMPORTANCE OF MAGNETIC FIELDS IN THE INTERSTELLAR MEDIUM

The results are part of a growing body of observational evidence that magnetic fields play a crucial role in the dynamics of interstellar gas in a variety of environments. For example, Troland and Heiles (1982*b*) suggest that the field limits density enhancements within cool postshock gas in large H I shells, and it may affect the overall dynamics of the shell itself. Heiles and Troland (1982) find that the field is likely to play an important role in the H I and molecular clouds in the Orion region, and Schwarz *et al.* (1986) draw a similar conclusion for the clumps of H I gas in the direction of Cas A.

The H I absorbing region in front of Orion A is one of several regions where field strengths are now known to be of order 100 μG or more. Other are the OH absorbing regions in front of Orion A (125 ± 20 μG, Troland *et al.*), S88B (69 ± 5 μG, Crutcher *et al.*), S106 (137 ± 20 μG, Kazès *et al.* 1988), and W3 (73 ± 7 μG, with some uncertainty owing to maser contamination, Kazès and Crutcher 1986). Fields this high must have significant effects upon the dynamics of the regions they permeate. Moreover, all of these regions are associated with molecular clouds in which massive star formation has occurred. In other molecular regions without massive star formation, field strengths appear to be considerably less, of order 20 to 30 μG (Crutcher *et al.*). Observations of interstellar magnetic fields are still sparse, yet the impression given by results so far is that the field mediates much of the process whereby interstellar clouds are formed, collapse, and give birth to new stars of various types. The Orion region, with its proximity and its diversity of environments, provides an excellent opportunity to study these effects.

This research was supported in part by an NSF grant to C. H., by NSF grant AST-8611887 to T. H. T., and by travel support for T. H. T. provided by the Netherlands Foundation for Radio Astronomy and the University of Groningen. We thank P. van der Werf and the referee for their useful comments on the manuscript.

REFERENCES

Ahmad, I. A. 1976, *Ap. J.*, **209**, 462.
Appenzeller, I. 1974, *Astr. Ap.*, **36**, 99.
Bohlin, R. C., Savage, B. D., and Drake, J. F. 1978, *Ap. J.*, **224**, 132.
Boughton, W. L. 1978, *Ap. J.*, **222**, 517.
Breger, M. 1976, *Ap. J.*, **204**, 789.
Brooks, J. W., Murray, J. D., and Radhakrishnan, V. 1971, *Ap. Letters*, **8**, 121.
Chaisson, E. J., and Dopita, M. A. 1977, *Astr. Ap.*, **56**, 385.
Crutcher, R. M., and Kazès, I. 1983, *Astr. Ap.*, **125**, L23.
Crutcher, R. M., Kazès, I., and Troland, T. H. 1987, *Astr. Ap.*, **181**, 119.
Dopita, M. A., Isobe, S., and Meaburn, J. 1975, *Ap. Space Sci.*, **34**, 91.
Gordon, C. P. 1970, *A.J.*, **75**, 914.
Goss, W. M. 1968, *Ap. J. Suppl.*, **15**, 131.
Heiles, C. 1987*a*, paper presented at the Summer School on Interstellar Processes, Jackson Hole, Wyoming, 1986 July.
———. 1987*b*, paper presented at the NATO Advanced Study Institute, Irsee, Federal Republic of Germany, 1986 August.
———. 1988, *Ap. J.*, **324**, 321.
Heiles, C., and Stevens, M. 1986, *Ap. J.*, **301**, 331.
Jaffee, D. T., and Pankonin, V. 1978, *Ap. J.*, **226**, 869.
Johnston, K. J., Palmer, P., Wilson, T. L., and Bieging, J. H. 1983, *Ap. J. (Letters)*, **271**, L89.
Kazès, I., and Crutcher, R. M. 1986, *Astr. Ap.*, **164**, 328.
Kazès, I., Troland, T. H., Crutcher, R. M., and Heiles, C. 1988, submitted to *Ap. J.*
Lee, T. A. 1968, *Ap. J.*, **152**, 913.
Lockhart, I. A., and Goss, W. M. 1978, *Astr. Ap.*, **67**, 355 (L&G).
Lockman, F. J., and Brown, R. L. 1975, *Ap. J.*, **201**, 134.
Maddalena, R. J., Morris, M., Moscowitz, J., and Thaddeus, P. 1986, *Ap. J.*, **303**, 375.
Martin, A. H. M., and Gull, S. F. 1976, *M.N.R.A.S.*, **175**, 235.
Mathewson, D. S., and Ford, V. L. 1970, *Mem. Roy. Astr. Soc.*, **74**, 139.
Mouschovias, T. Ch. 1976*a*, *Ap. J.*, **206**, 753.
———. 1976*b*, *Ap. J.*, **207**, 141.
Mouschovias, T. Ch., Shu, F. H., and Woodward, P. R. 1974, *Astr. Ap.*, **33**, 73.
O'Dell, C. R., and Hubbard, W. B. 1965, *Ap. J.*, **142**, 591.
Parker, E. N. 1966, *Ap. J.*, **145**, 811.
Qaiyum, A., and Razaullah Ansari, S. M. 1983, *M.N.R.A.S.*, **205**, 719.
Savage, B. D., Bohlin, R. C., Drake, J. F., and Budich, W. 1977, *Ap. J.*, **216**, 291.
Savage, B. D., and Jenkins, E. B. 1972, *Ap. J.*, **172**, 491.
Schwarz, U. J., Troland, T. H., Albinson, J. S., Bregman, J. D., Goss, W. M., and Heiles, C. 1986, *Ap. J.*, **301**, 320.
Shaver, P. A. 1980, *Astr. Ap.*, **90**, 34.
Simard-Normandin, M., and Kronberg, P. P. 1980, *Ap. J.*, **242**, 74.
Terzian, Y., and Parrish, A. 1970, *Ap. Letters*, **5**, 261.
Troland, T. H., and Heiles, C. 1982*a*, *Ap. J.*, **252**, 179.
———. 1982*b*, *Ap. J. (Letters)*, **260**, L19.
———. 1986, *Ap. J.*, **301**, 339.
Troland, T. H., Crutcher, R. M., and Kazès, I. 1986, *Ap. J. (Letters)*, **304**, L57.

Verschuur, G. L. 1969, *Nature*, **223**, 140.
Walmsley, C. M. 1975, in *H II Regions and Related Topics*, ed. T. L. Wilson and D. Downes (New York: Springer), p. 17.
Wilson, T. L., and Jäger, B. 1987, *Astr. Ap.*, **184**, 291.
Wilson, T. L., and Pauls, T. 1984, *Astr. Ap.*, **138**, 225.
Zuckerman, B., and Ball, J. A. 1974, *Ap. J.*, **190**, 35.
Zuckerman, B., Palmer, P., and Rickard, L. J. 1975, *Ap. J.*, **197**, 571.

W. M. Goss: National Radio Astronomy Observatory, P.O. Box 0, Socorro, NM 87801

C. Heiles: Astronomy Department, University of California, Berkeley, CA 94720

T. H. Troland: Physics and Astronomy Department, University of Kentucky, Lexington, KY 40506